IAC–17–B2.5.9.x39317

Inertially Aided Vector Matching for Opportunistic Navigation in Space

Joel Runnels [a*], **Demoz Gebre-Egziabher** [b]

[a] *Aerospace Engineering and Mechanics Department, University of Minnesota, 110 Union Street SE Minneapolis, Minnesota, United States, runne010@umn.edu*
[b] *Aerospace Engineering and Mechanics Department, University of Minnesota, 110 Union Street SE Minneapolis, Minnesota, United States, gebre@umn.edu*
[*]Corresponding Author

Abstract

In this work, an estimator is developed for the joint estimation of orientation and position from astrophysical signals of opportunity, particularly pulsars. The filter is based on a combination of vector-matching techniques for estimating attitude and time-difference of arrival navigation for estimating position. The filter functions by computing the probability of association for each arriving photon with each signal source of interest, and using the association probabilities to perform the measurement update. The probability of association of a photon with a signal source is derived, as well as the probability of association with background. The estimation techniques proposed are tested using Monte Carlo analysis techniques. The accuracy of the resulting estimates is compared to other pulsar navigation techniques. The results of the simulation studies indicate that the technique proposed here generally outperforms other time difference of arrival estimation techniques.
Keywords: Opportunistic navigation, data association

Nomenclature

State Estimation

j, k	=	Time indices
$\hat{\mathbf{x}}$	=	State vector
m	=	State vector dimension
$\mathbf{P}$	=	State vector covariance matrix
$\mathbf{H}$	=	Measurement matrix
$\mathbf{K}$	=	Kalman gain matrix
y	=	Measurement values
v	=	Measurement noise
$\mathbf{R}$	=	Variance of measurement noise
δy	=	Measurement residual
$\mathbf{S}$	=	Variance of measurement residual

Navigation Symbols

$\mathbf{r}$	=	Position vector
$\mathbf{q}$	=	Attitude vector
θ	=	Orientation angle (1DOF)
$\bar{u}$	=	Unit vector
$\mathbf{C}_A^B(\cdot)$	=	Direction cosine matrix to transform vector from frame A to frame B, as a function of attitude information $(\cdot)$
N	=	Navigation frame
B	=	Body frame

Photon Arrival and Flux

$\tilde{\lambda}$	=	Time-binned photon arrivals
t	=	Photon time of arrival
$\boldsymbol{\alpha}$	=	Photon angle of arrival
$\lambda_N^{(S)}(t)$	=	Photon flux (in photons/second) of signal S at time t at location N
$\lambda_{N,k}^{(S)}$	=	Expected number of photons from signal S over time-bin k at origin of frame N
S^p	=	Signal of opportunity
A_p	=	The event that a given photon originated from source S^p
$\mathbf{A}$	=	The set of all possible associations
β_p	=	The probability that a given photon originated from source S^p
c	=	Speed of light

Statistics Symbols

$\mathbf{Pr}[\cdot]$	=	Probability of event $(\cdot)$
$\mathrm{var}(\cdot)$	=	Variance of $(\cdot)$
$\mathbb{E}[\cdot]$	=	Expected value of $(\cdot)$
$c_{a,b}[t]$	=	Correlation between signal A and signal B at time-offset t
T	=	Time-step between taps in correlation vector

Bold-faced symbols denote a vector.

Acronyms/Abbreviation

AOA	=	Angle of arrival
DOF	=	Degree of freedom
DSN	=	Deep Space Network
GEO	=	Geosynchronous Earth orbit
GRB	=	γ-ray burst
LEO	=	Low Earth orbit
MLE	=	Maximum likelihood estimator
MSP	=	Millisecond pulsar
NHPP	=	Non-homogeneous Poisson process
PDF	=	Probability density function
PNT	=	Position, navigation and timing
SNR	=	Signal to noise ratio
SOP	=	Signal of opportunity
TDOA	=	Time-difference of arrival
TOA	=	Time of arrival

1. Introduction

Many envisioned future missions for small satellites (micro and picosats) will require operation in deep space which, for the purposes of this paper, is defined to be distances of 1.0 AU or more from Earth. Autonomous navigation and time synchronization capability for small satellites in deep space is virtually non-existent. Many off-the-shelf solutions for small satellites and CubeSats assume operations in Earth orbit where signals from GPS or other Global Navigation Satellite Systems (GNSS) are available. This has been the motivation for several current research efforts aimed at determining how to make opportunistic use of signals (photons) emitted by celestial x-ray and gamma-ray sources (pulsar, quasars, gamma-ray bursts). Since these signals are ubiquitous, a navigation system that uses these signals can provide services anywhere in the solar system. When pulsars are the signal of opportunity, individual spacecraft to determine their position and synchronize their clocks relative to the solar system barycenter. When using non-periodic signals emanating from quasars or gamma-ray bursts, this approach allows for relative ranging and clock synchronization between pairs or a swarm of cooperating small satellites.

As a reference mission to highlight the technological gap filled by this approach to navigation we consider Near Earth Asteroid Scout (NEA Scout). The vehicle used by NEA Scout will be a 3U CubeSat equipped with a science-grade monochromatic camera augmented by color strip (static) filter. It will perform a near flyby (within 10 km) of a target asteroid at a distance of approximately 1 AU from Earth. Camera images collected during the flyby will be used to characterize the asteroid and assess its suitability for subsequent human exploration. NEA Scout will develop technologies and retire risks needed for the capability to autonomously scout Near Earth Asteroids identified by the Human Exploration and Operations Mission Directorate (HEOMD) as potential targets for future human exploration. For navigation and communication, NEA Scout will leverage technology developed by other deep space CubeSat missions namely INSPIRE and MarCO. With respect to navigation and communication, NEA Scout will use the IRIS X-band transponder. The transponder will allow communications with the Deep Space Network (DSN) on Earth. The DSN will be used for localizing the CubeSat.

DSN is a reliable technology which can provide accurate positioning. However, its accuracy comes at a cost of operational flexibility. This is because the accuracy it can provide in cross track positioning (angular resolution) depends on the length of measurement time [1, 2]. In the future where fleets of CubeSats are envisioned to be operating in deep space this can be untenable. Unlike DSN, the positioning solution generated by when using pulsar is continuous.

1.1 Prior Work

The idea of using celestial signal sources for positioning is as old as the seafaring tradition of humans. Using astrophysical signals for navigation in deep space is a reincarnation of that same idea. In this regard, [3] and [4] seminal works that showed how x-ray pulsars can be used for navigation. Follow work in [5–11] examined various algorithm details for positioning using pulsars. A central finding in all of these works was that the signal-to-noise ratio (SNR) of pulsar signals are rather small and, thus, require x-ray detectors with larger area. In [12] analysis was presented that showed a $1000\text{cm}^2 2$ detector area could yield a position solution to with accuracy on the order of 10 km. To deal with the low SNR problem, [13] considered the problem when using signals emanating from Gamma Ray Bursts (GRB). While the use of GRBs alleviates the problem associated with SNR to some extent, the fact that these signals are sporadic in time limits their utility for continuous positioning applications.

In addition to the SNR problem, there is a secondary challenge that needs be addressed but that has not received much attention. This is the problem of data association; for every x-ray photon received, we need to be able to determine which pulsar it emanated from. This problem couples the attitude of the detector (and, by extension, the space vehicle) with the positioning problem. To this end,

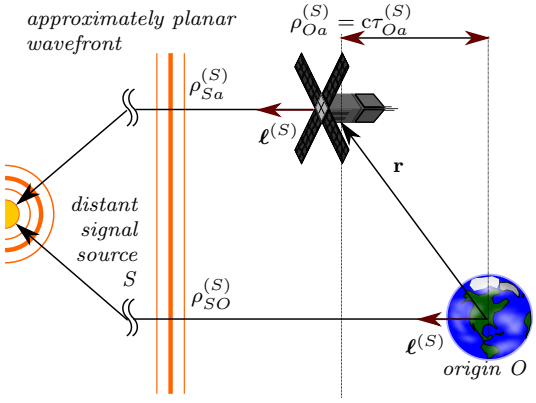

Fig. 1: Absolute NAVSOP concept

this paper presents a data association filter which allows simultaneous estimation of attitude and position using x-ray signals from pulsars.

1.2 Paper Organization

The presentation of the problem in this paper is structured as follows: First, a review of positioning using signals from pulsars is briefly reviewed. This will provide some of the foundation required to understand the derivation of the data association filter that is presented next. This will be followed by a presentation of results from a series of simulation studies performed to assess the performance of the data association filter. A conclusion summarizing the papers results and providing suggestions for future closes the paper.

2. NAVSOP Basic Concepts

The basic idea behind x-ray pulsar navigation is to estimate the time of arrival (TOA) of pulses from several pulsars at the spacecraft. These TOAs are then compared to the TOA of the same pulses at Earth. The difference between the arrival times gives the time-difference of arrival (TDOA) for each pulsar signal. From these TDOAs, a position, navigation and timing solution may be computed. Figure 1 illustrates this principle. A basic measurement update equation that would be used in such a navigation scheme is given below:

$$\mathbf{y}(\mathbf{x}) = \begin{bmatrix} \tau_{Oa}^{(1)} \\ \vdots \\ \tau_{Oa}^{(N)} \end{bmatrix} = \begin{bmatrix} -\frac{1}{\mathrm{c}} \left(\boldsymbol{\ell}^{(1)}\right)^T & 1 \\ \vdots & \\ -\frac{1}{\mathrm{c}} \left(\boldsymbol{\ell}^{(N)}\right)^T & 1 \end{bmatrix} \begin{bmatrix} \mathbf{r}^{(Oa)} \\ \delta t_a \end{bmatrix} \quad (1)$$

Since the pulse profiles and timing characteristics of many millisecond pulsars (MSPs) are highly stable, the pulse TOAs at Earth can be known *a priori*, and stored on-board the spacecraft computer. As a result, the TDOA may be computed on-board the spacecraft without any communication with Earth. This principle is similar to the basic principle used in GPS navigation.

3. Joint Estimation

The goal of the estimator proposed here is to estimate the time difference of arrival (TDOA) for an arbitrary number of astrophysical x-ray signals of opportunity, as well as the attitude of the detector, based on photon time of arrival (TOA) and angle of arrival (AOA) measurements. In previous work, an estimator was developed for estimation of TDOA for a single signal of opportunity, specifically signals from x-ray pulsars [12]. The estimator functions by estimating the correlation vector between the signal measured by the detector, and the known pulse profile at the navigation origin. The TDOA for that signal could then be estimated by estimating the location of the peak of the correlation function.

This estimator extends the technique discussed above to multiple signals of opportunity, in which the origin of the arriving photons is not well known.

4. Single Correlation Vector

For completeness, the estimator used to estimate a single correlation vector is summarized here.

The expected value of the state vector is equal to the correlation between the measured signal and the signal at the navigation frame origin. Mathematically:

$$\mathbb{E}\left[\hat{\mathbf{x}}_k\left[p\right]\right] = c_{\lambda,\lambda_O}\left[p\right] = \sum_i \lambda_{k+i}\lambda_{O,k+i+p} \quad (2)$$

where

- λ_k is the expected number of photons at time index k at the detector
- $\lambda_{O,k}$ is the expected number of photons at time index k at the navigation frame origin

It may be shown that for very weak signals, the correlation vector is also equal to the ideal finite impulse response (FIR) filter for reconstructing the true signal from the weak version of the signal. Consequently, the measurement update for the correlation vector may be written as follows.

$$\begin{aligned} y_k = \lambda_{O,k} &= h(\hat{\mathbf{x}}_k\ , \boldsymbol{\Lambda}_k, \mathbf{v}_{\mathrm{Pois}}) \\ &= \tilde{\boldsymbol{\Lambda}}_k^T\ \hat{\mathbf{x}}_k \\ &= \left(\boldsymbol{\Lambda}_k + \mathbf{v}_{\mathrm{Pois}}\right)^T\ \hat{\mathbf{x}}_k \end{aligned} \quad (3)$$

where $\tilde{\mathbf{\Lambda}}_k$ is a vector consisting of the last n time-binned photon counts.

The measurement residual associated with the measurement update is given by

$$\mathbf{S_c} = \tilde{\mathbf{\Lambda}}_k \mathbf{P}_k^- \tilde{\mathbf{\Lambda}}_k^T + \lambda_k \, \hat{\mathbf{x}}_k \, \hat{\mathbf{x}}_k{}^T \tag{4}$$

An alternative formulation of the measurement update equations makes use of the fact that the photon arrivals for a given signal are very sparse. Thus, the photon arrival vector $\tilde{\mathbf{\Lambda}}_k$ usually consists of all zeros, or zeros and a single one. After a photon arrival, the photon arrival vector takes the following form.

$$\begin{aligned} \tilde{\mathbf{\Lambda}}_k &= \begin{bmatrix} 1 & 0 & 0 & \dots & 0 \end{bmatrix} \\ \tilde{\mathbf{\Lambda}}_{k+1} &= \begin{bmatrix} 0 & 1 & 0 & \dots & 0 \end{bmatrix} \\ \tilde{\mathbf{\Lambda}}_{k+2} &= \begin{bmatrix} 0 & 0 & 1 & \dots & 0 \end{bmatrix} \\ \tilde{\mathbf{\Lambda}}_{k+n-1} &= \begin{bmatrix} 0 & 0 & 0 & \dots & 1 \end{bmatrix} \end{aligned} \tag{5}$$

It is apparent that after a photon arrives, each tap in the correlation vector will be updated sequentially. Alternatively, all taps can be updated at once using the following expression.

$$\begin{aligned} \mathbf{y}_k = \mathbf{\Lambda}_{O,k} &= \mathbf{h}(\hat{\mathbf{x}}_k \, , \mathbf{\Lambda}_k, \mathbf{v}_{\text{Pois}}) \\ &= (\mathbf{I}_{n\times n}(1 + v_{\text{Pois}}))^T \, \hat{\mathbf{x}}_k \end{aligned} \tag{6}$$

The resulting measurement residual is simply:

$$\boldsymbol{\delta}\mathbf{y_c} = \mathbf{\Lambda}_{O,k} - \hat{\mathbf{x}}_k \tag{7}$$

The variance of the measurement residual is given by:

$$\mathbf{S_c} = \mathbf{P}_k^- + \mathbf{I}_{n\times n} \left(\lambda_k \, \hat{\mathbf{x}}_k \, \hat{\mathbf{x}}_k{}^T \right) \tag{8}$$

5. The State Vector

In [12], the state vector consists of the correlation function values at various delays between the measured signal, consisting of the measured photons, and the signal at the navigation frame origin. In this work, the state vector consists of multiple correlation vectors, one for each signal source being tracked, as well as an attitude estimate. The state vector is written as follows:

$$\hat{\mathbf{x}} = \begin{bmatrix} \hat{\mathbf{c}}_{\tilde{\lambda},S^0} \\ \hat{\mathbf{c}}_{\tilde{\lambda},S^1} \\ \vdots \\ \hat{\mathbf{c}}_{\tilde{\lambda},S^N} \\ \hat{\mathbf{q}} \end{bmatrix} \tag{9}$$

where

- $\mathbf{c}_{\tilde{\lambda},S^N}$ is the correlation between the photon arrivals at the detector, $\tilde{\lambda}$, and the signal being tracked at the navigation frame origin, λ_O
- $\mathbf{q}$ is the vector containing the attitude quaternion of the detector

6. Data Association

When a photon hits the detector, the two measurable quantities are time of arrival and angle of arrival relative to the detector. It is not immediately obvious from which signal source the photon originated, or whether it originated from background x-ray flux. If the orientation of the detector is known to a high degree of accuracy, then it is easier to associate a given photon with a signal source based on angle of arrival. Even if the orientation is known perfectly however, it is still not possible to determine with certainty whether the photon originated from a SOP or from x-ray background.

Because it is not possible to determine with complete certainty the origin of a given x-ray photon, it is not always clear which correlation vector should be updated, if any. To address this problem, the probabilistic data association filtering technique is used to simultaneously update all of the correlation vectors based on the probability that the photon originated from each given signal source.[14, 15]

In order to perform this update, the probability of the photon originating from each signal source must be computed. This estimator uses a similar expression for the computation of association probabilities to what is presented in [14], adapted to the specific case of photon arrivals. The probability is computed using Bayes' rule as shown below.

$$\beta_p = \mathbf{Pr}\left[A_p | t_i, \boldsymbol{\alpha}_i\right] = \frac{\mathbf{Pr}\left[t_i, \boldsymbol{\alpha}_i | A_p\right] \mathbf{Pr}\left[A_p\right]}{\mathbf{Pr}\left[t_i, \boldsymbol{\alpha}_i\right]} \tag{10}$$

where

- A_p is the event in which photon i originated from from signal p
- t_i is the time of arrival of photon i
- $\boldsymbol{\alpha}_i$ is the angle of arrival of photon i, in the detector coordinate frame (local coordinates)

The analytical expression for each term in Equation 10 is derived below.

6.1 Measurement Probability

In this section, the probability of a photon originating from source S^p arriving at time t_i and angle $\boldsymbol{\alpha}_i$ is computed. This is the term $\mathbf{Pr}\left[t_i, \boldsymbol{\alpha}_i | A_p\right]$ in equation 10. In this work, the signal sources are

assumed to be point sources. Therefore, the angle of arrival is dependent only upon the orientation of the detector and the measurement error in AOA measurement. With these assumptions, the angle of arrival and time of arrival may be considered statistically independent. This allows the joint probability to be written as follows.

$$\mathbf{Pr}\left[t_i, \boldsymbol{\alpha}_i | A_p\right] = \mathbf{Pr}\left[\boldsymbol{\alpha}_i | A_p\right] \mathbf{Pr}\left[t_i | A_p\right] \tag{11}$$

6.1.1 Angle Of Arrival Probability

The probability of a photon from source S^p arriving at angle $\boldsymbol{\alpha}_i$ is computed from the probability distribution function of the angle measurement residual.

The formulation of the angle measurement residual is taken from vector-matching estimation techniques, such as [16]. The attitude measurement residual is the difference between the unit vector to the signal source in the body frame, and the unit vector of the arriving photon. The residual is written as:

$$\boldsymbol{\delta}\mathbf{y}_\mathbf{q} = \mathbf{C}_N^B(\hat{\mathbf{q}})\bar{u}_p^N - \bar{u}_i^B \tag{12}$$

where

- $\mathbf{C}_N^B(\hat{\mathbf{q}})$ is the direction cosine matrix which transforms vectors from the navigation frame to the body frame, based on the current attitude estimate $\hat{\mathbf{q}}$
- $\bar{u}_p^N$ is the unit vector of the signal source p in the navigation frame
- $\bar{u}_i^B$ is the unit vector of the arriving photon i in the body frame

The attitude measurement matrix, $\mathbf{H}_\mathbf{q}$ is written as

$$\mathbf{H}_\mathbf{q} = \left[-2\left(\mathbf{C}_N^B(\hat{\mathbf{q}})\bar{u}_p^N\right)^\times\right] \tag{13}$$

as derived in detail in [16].

Given the measurement residual, and the measurement residual covariance, the relative likelihood of that measurement residual having originated from the current signal source of interest may be computed using the normal probability density function.

$$\mathbf{Pr}\left[\boldsymbol{\alpha}_i | A_p\right] = \mathcal{N}\left[\boldsymbol{\delta}\mathbf{y}, \mathbf{S}\right] \tag{14}$$

where $\mathbf{S}_\mathbf{q} = \mathbf{H}_\mathbf{q}\mathbf{P}^-\mathbf{H}_\mathbf{q}^T + \mathbf{R}_\mathbf{q}$ is the measurement residual covariance matrix

6.1.2 Time Of Arrival Probability

The likelihood of a photon from a given signal source arriving at a specific time is dependent on the estimated photon flux rate from the signal source at that instant in time. The arrival of x-ray photons is a non-homogeneous Poisson process (NHPP), i.e. a Poisson process where the rate of arrival varies as a function of time.

The probability of the photon arriving at a specific time must be computed, given that a photon did in fact originate from the signal source, (i.e. given that A_p is true). Photon arrivals from a signal source with time-varying intensity governed by a non-homogeneous Poisson process. The arrival times between events in a non-homogeneous Poisson process can be modeled as follows [17].

$$\mathbf{Pr}\left[t|\lambda(t)\right] = \max[\lambda]e^{-\max[\lambda]t}\frac{\lambda(t)}{\max[\lambda]} \tag{15}$$

Applied to the photon arrival problem, the probability distribution function for the arrival time of a photon from signal S^p may be written as follows.

$$\begin{aligned}\mathbf{Pr}\left[t_i|A_p\right] &\sim \max[\lambda]e^{-\max[\lambda]t_i}\frac{\lambda(t_i)}{\max[\lambda]} \\ &= e^{-\max[\lambda]t_i}\lambda(t_i) \\ &= e^{-\max[\lambda_O]t_i}\lambda_O(t_i + \hat{\tau}^{(S)})\end{aligned} \tag{16}$$

The last two lines in Equation 16 reflect the fact that λ is equal to λ_O delayed by $\tau^{(S)}$. The term $\hat{\tau}^{(S)} = \hat{\mathbf{r}}_{t_i} \cdot \boldsymbol{\ell}^{(p)}$ is the signal's TDOA. This term is not well-known, but rather is a quantity to be estimated. Since the TDOA is not known, the flux from the signal source is not known exactly either. Since the flux function λ is not linear, it is not sufficient to compute the flux directly from the estimate of TDOA. Rather, the expected value must be taken.

Given the mean and variance of the TDOA estimate, the expected value of the flux would be computed as follows:

$$\mathbb{E}\left[\lambda_O(t_i + \hat{\tau}^{(S)})\right] = \int_{-\infty}^{\infty}\lambda_O(t)f(t|\tau, \sigma_\tau^2)dt \tag{17}$$

where $f(t|\tau, \sigma_\tau^2)$ is the PDF of the normal distribution. This integral cannot be directly computed, so instead the following approximation is used.

$$\begin{aligned}
&\mathbb{E}\left[\lambda_O(t_i+\hat{\tau}^{(S)})\right] \\
&\approx \frac{1}{\sqrt{12}\sigma_\tau}\int_{t_i+\hat{\tau}-\sqrt{3}\sigma_\tau}^{t_i+\hat{\tau}+\sqrt{3}\sigma_\tau}\lambda_O(t_i+t)dt \\
&= \frac{F_{\lambda_O}(t_i+\hat{\tau}+\sqrt{3}\sigma_\tau)-F_{\lambda_O}(t_i+\hat{\tau}-\sqrt{3}\sigma_\tau)}{\sqrt{12}\sigma_\tau} \\
&= \frac{F_{\lambda_O}|_{t_i+\hat{\tau}-\sqrt{3}\sigma_\tau}^{t_i+\hat{\tau}+\sqrt{3}\sigma_\tau}}{\sqrt{12}\sigma_\tau}
\end{aligned} \tag{18}$$

where $F_{\lambda_O} = \int \lambda_O(t)dt$ is the indefinite integral of the flux profile with respect to time.

This expression is the result of approximating the normally distributed TDOA as a uniform distribution with variance equal to that of the original normal distribution. The integral in the approximation above is easily obtained because the indefinite integral can be numerically computed once for each signal source. The results of this indefinite integral can then be used to compute the definite integral. The final expression for the approximate arrival time probability is given below.

$$\mathbf{Pr}\left[t_i|A_p\right] \approx e^{-\lambda_{\max}t_i}\frac{F_\lambda|_{t_i+\hat{\tau}-\sqrt{3}\sigma_\tau}^{t_i+\hat{\tau}+\sqrt{3}\sigma_\tau}}{\sqrt{12}\sigma_\tau} \tag{19}$$

In summary, the probability of measuring a photon at angle of arrival $\boldsymbol{\alpha}_i$ and time of arrival t_i is given by:

$$\begin{aligned}
&\mathbf{Pr}\left[\boldsymbol{\alpha}_i, t_i|A_p\right] \approx \\
&\mathcal{N}\left[\boldsymbol{\delta}\mathbf{y}, \mathbf{S}\right] e^{-\lambda_{\max}t_i}\frac{F_\lambda|_{t_i+\hat{\tau}-\sqrt{3}\sigma_\tau}^{t_i+\hat{\tau}+\sqrt{3}\sigma_\tau}}{\sqrt{12}\sigma_\tau}
\end{aligned} \tag{20}$$

6.1.3 Background Probability

The probabilities computed above have been for the case in which the photon is associated with a time-varying signal source. The other possible outcome is that the photon originates from the ambient x-ray background. For this association event, the probability of the given angle and time of arrival must also be computed.

$$\mathbf{Pr}\left[\boldsymbol{\alpha}_i, t_i|A_{\text{bkg}}\right] = \mathbf{Pr}\left[\boldsymbol{\alpha}_i|A_{\text{bkg}}\right]\mathbf{Pr}\left[t_i|A_{\text{bkg}}\right] \tag{21}$$

Background photon arrivals are assumed to be uniformly distributed in angle of arrival. Consequently, the PDF of the angle of arrival of a background photon is expressed as follows.

$$\mathbf{Pr}\left[\boldsymbol{\alpha}_i|A_{\text{bkg}}\right] \sim \frac{1}{V} \tag{22}$$

where V is the region of observation.

The arrival times of background x-ray photons are governed by the exponential distribution. Background photons are assumed to arrive at a constant rate. Therefore, the PDF of the background photon arrival times is given as follows.

$$\mathbf{Pr}\left[t_i|A_{\text{bkg}}\right] \sim \lambda^{(\text{bkg})}e^{\lambda^{(\text{bkg})}t_i} \tag{23}$$

6.2 Association Probability

The probability of observing a photon associated with signal source S^p, $\mathbf{Pr}\left[A_p\right]$ will now be computed. This is a discrete random variable, and the probability of each outcome may be directly computed from the relative average signal strengths of each signal source.

$$\mathbf{Pr}\left[A_p\right] = \frac{\mathbb{E}\left[\lambda^{(p)}\right]}{\lambda^{(\text{bkg})}+\sum_{i=1}^{N}\mathbb{E}\left[\lambda^{(i)}\right]} \tag{24}$$

Similarly, the probability of seeing a photon from the ambient x-ray background may be computed as follows.

$$\mathbf{Pr}\left[A_{\text{bkg}}\right] = \frac{\lambda^{(\text{bkg})}}{\lambda^{(\text{bkg})}+\sum_{i=1}^{N}\mathbb{E}\left[\lambda^{(i)}\right]} \tag{25}$$

The final term in Equation 10 is the denominator, $\mathbf{Pr}\left[t_i, \boldsymbol{\alpha}_i\right]$. However, since this term appears the same in the probability of every association event, and since the total of all the association probabilities must sum to zero, this term does not need to be computed. Rather, it can be accounted for as a constant which is set such that the probabilities sum to one.

In summary, the probability of association with a given signal source may be written as follows.

$$\begin{aligned}
\beta_p &= \frac{\mathcal{N}\left[\boldsymbol{\delta}\mathbf{y}, \mathbf{S}\right] e^{-\max[\lambda^{(p)}]t_i}\; F_{\lambda^{(p)}}|_{t_i-\sqrt{3}\sigma_\tau}^{t_i+\sqrt{3}\sigma_\tau}}{c\left(\lambda^{(\text{bkg})}+\sum_{i=1}^{N}\mathbb{E}\left[\lambda^{(i)}\right]\right)\sqrt{12}\sigma_\tau} \\
\beta_{\text{bkg}} &= \frac{\frac{1}{V}\lambda^{(\text{bkg})}e^{-\lambda^{(\text{bkg})}t_i}}{c\left(\lambda^{(\text{bkg})}+\sum_{i=1}^{N}\mathbb{E}\left[\lambda^{(i)}\right]\right)}
\end{aligned} \tag{26}$$

where c is a constant defined such that the sum of the probabilities is one.

7. Measurement Update

Having computed the association probabilities for each possible photon association, the next task is to update the state vector accordingly. The state update procedure performed here follows the state update procedure outlined in [14, 15].

Due to the uncertainty in the origin of any given photon, the true distribution of the state vector

after an update consists of a Gaussian mixture. In general terms, the *a posteriori* distribution of the state vector can be described as follows.

$$\hat{\mathbf{x}}_k^+ \sim \beta_{\text{bkg}}\mathcal{N}\left[\hat{\mathbf{x}}_k^- \ , \mathbf{P}_k^-\right] + \sum_{i=1}^{N}\beta_i\mathcal{N}\left[\hat{\mathbf{x}}_{k|A_i}^+ \ , \mathbf{P}_{k|A_i}^+\right] \tag{27}$$

In other words, the state vector after a photon arrives is distributed according to a Gaussian mixture composed of a sum of the resulting distributions from each possible photon association.

While this is the true distribution, it is impossible to actually keep track of each term in the mixture, since after each photon arrival the number of terms grows is multiplied by the number of possible association events, i.e. $N+1$. Consequently, after i photon arrivals, the state vector PDF would consist of an $(N+1)^i$-component mixture. Given that thousands of photon observations are required to obtain an accurate TDOA estimate, it is clearly intractable to keep track of the true Gaussian mixture.

The joint probability data association filter addresses the Gaussian mixture problem by approximating the resulting mixture as a single Gaussian. This is the key assumption of this estimation scheme. The probabilistic data association filter approximates the Gaussian mixture using the moment matching technique, as outlined in [18, Section 1.4.16].

It may be shown that, for a Gaussian mixture, the following properties hold.

$$f(x) = \sum_{i=1}^{n} w_i\mathcal{N}\left[\mu_i, \sigma_i^2\right] \tag{28a}$$

$$\mathbb{E}\left[x\right] = \sum_{i=1}^{n} w_i\mu_i \tag{28b}$$

$$\text{var}\left(x\right) = \sum_{i=1}^{n} w_i\left(\sigma_i^2 + \left(\mu_i - \mathbb{E}\left[x\right]\right)^2\right) \tag{28c}$$

In the joint probability data association filter, these properties are used to compute a Gaussian distribution in which the mean and variance is matched to the mean and variance of the Gaussian mixture. The details of implementation in the case of TDOA and attitude estimation are outlined below.

For a given photon, the probability of association with each signal source as well as background noise is computed, as outlined in Section 6. Then, for each association event, a measurement matrix and measurement residual are computed, assuming that the given association event is correct. These measurement residuals are then stacked to form a single weighted measurement residual vector:

$$\delta y_{k|\mathbf{A}} = \begin{bmatrix} \beta_1\boldsymbol{\delta}\mathbf{y}_{c_{\tilde{\lambda},S^1}} \\ \beta_1\boldsymbol{\delta}\mathbf{y}_{\mathbf{q}|A_1} \\ \beta_2\boldsymbol{\delta}\mathbf{y}_{c_{\tilde{\lambda},S^2}} \\ \beta_2\boldsymbol{\delta}\mathbf{y}_{\mathbf{q}|A_2} \\ \vdots \\ \beta_N\boldsymbol{\delta}\mathbf{y}_{c_{\tilde{\lambda},S^N}} \\ \beta_N\boldsymbol{\delta}\mathbf{y}_{\mathbf{q}|A_N} \end{bmatrix} = \begin{bmatrix} \beta_1\left(\boldsymbol{\Lambda}_O - \hat{\mathbf{c}}_{\tilde{\lambda},S^1}\right) \\ \beta_1\mathbf{C}_N^B(\hat{\mathbf{q}})\bar{u}_1^N - \bar{u}_1^B \\ \beta_2\left(\boldsymbol{\Lambda}_O - \hat{\mathbf{c}}_{\tilde{\lambda},S^2}\right) \\ \beta_2\mathbf{C}_N^B(\hat{\mathbf{q}})\bar{u}_2^N - \bar{u}_2^B \\ \vdots \\ \beta_N\left(\boldsymbol{\Lambda}_O - \hat{\mathbf{c}}_{\tilde{\lambda},S^N}\right) \\ \beta_N\mathbf{C}_N^B(\hat{\mathbf{q}})\bar{u}_N^N - \bar{u}_N^B \end{bmatrix} \tag{29}$$

Similarly, the measurement matrices corresponding to each measurement association are also stacked to form a single measurement matrix.

$$\begin{aligned} \mathbf{H}_{k|\mathbf{A}} &= \begin{bmatrix} \mathbf{H}_{A_1} \\ \mathbf{H}_{A_2} \\ \vdots \\ \mathbf{H}_{A_N} \end{bmatrix} \\ &= \begin{bmatrix} \mathbf{H}_{\mathbf{c}|A_1} & \mathbf{0} & \dots & \mathbf{0} \\ \mathbf{H}_{\mathbf{q}|A_1} & \mathbf{0} & \dots & \mathbf{0} \\ \mathbf{0} & \mathbf{H}_{\mathbf{c}|A_2} & \dots & \mathbf{0} \\ \mathbf{0} & \mathbf{H}_{\mathbf{q}|A_2} & \dots & \mathbf{0} \\ \vdots & \vdots & \ddots & \vdots \\ \mathbf{0} & \mathbf{0} & \dots & \mathbf{H}_{\mathbf{c}|A_N} \\ \mathbf{0} & \mathbf{0} & \dots & \mathbf{H}_{\mathbf{q}|A_N} \end{bmatrix} \end{aligned} \tag{30}$$

And finally, the measurement noise matrix is assembled in the same manner.

$$\mathbf{R}_{k|\mathbf{A}} = \begin{bmatrix} \mathbf{R}_{A_1} & \mathbf{0} & \dots & \mathbf{0} \\ \mathbf{0} & \mathbf{R}_{A_2} & \dots & \mathbf{0} \\ \vdots & \vdots & \ddots & \vdots \\ \mathbf{0} & \mathbf{0} & \dots & \mathbf{R}_{A_2} \end{bmatrix} \tag{31}$$

Having assembled these matrices, the state vector may be updated using the standard Kalman filtering equations.

$$\mathbf{S}_{k|\mathbf{A}} = \mathbf{R}_{k|\mathbf{A}} + \mathbf{H}_{k|\mathbf{A}}\mathbf{P}_k^-\mathbf{H}_{k|\mathbf{A}}^T \tag{32a}$$

$$\mathbf{K}_{k|\mathbf{A}} = \mathbf{P}_k^-\mathbf{H}_{k|\mathbf{A}}^T\mathbf{S}_{k|\mathbf{A}}^{-1} \tag{32b}$$

$$\hat{\mathbf{x}}_{k|\mathbf{A}}^+ = \hat{\mathbf{x}}_k^- + \mathbf{K}_{k|\mathbf{A}}\delta y_{k|\mathbf{A}} \tag{32c}$$

So far, we have computed the mean of the mixture, in keeping with Equation 28b, and set the updated state vector equal to that mean. The next task is to compute the covariance of the resulting mixture, which will serve as the covariance of the updated state.

Note from Equation 28c that it is not sufficient to simply take a weighted average of the covariances

of each mixture component. In order to match the variance of the Gaussian mixture that is being approximated, an additional term, referred to as the "spread of means" term must also be included. This term reflects the difference in the means of different mixture components.

Consequently, the covariance of the state vector after the measurement update and approximation is given by:

$$\mathbf{P}_k^+ = \sum_{i=1}^{N} \beta_i \left(\mathbf{P}_{k|A_i}^+ + (\hat{\mathbf{x}}_{k|\mathbf{A}}^+ - \hat{\mathbf{x}}_{k|A_i}^+)(\hat{\mathbf{x}}_{k|\mathbf{A}}^+ - \hat{\mathbf{x}}_{k|A_i}^+)^T \right) \tag{33}$$

7.1 Photon Validation

In theory, every photon that arrives at the detector could be used to update the state, as outlined above. However in practice, for a wide field-of-view detector, this may be impractical.

In a large detector with a wide field-of-view, the number of background photons which hit the detector could potentially be very large. The resulting probability of association with a signal source of interest would be very small for the vast majority of the photons (depending upon the accuracy with which position and attitude are known). However, the computational resources required to update the state vector are the same for each photon, regardless of its association probability. Therefore, it is beneficial from a computational standpoint to validate the photons initially before performing the state update.

In this estimation scheme, the photons are validated by computing the Mahalanobis distance for the attitude residual, following the technique for measurement validation presented in [14].

$$d_i = \sqrt{(\boldsymbol{\delta}\mathbf{y}_{\mathbf{q},i})^T \, \mathbf{S}_{\mathbf{q},i}{}^{-1} \, (\boldsymbol{\delta}\mathbf{y}_{\mathbf{q},i})} < \gamma \tag{34}$$

The validation threshold, γ corresponds to the probability that the validation region will contain a measurement from the signal source of interest. Choosing a high validation threshold ensures with greater probability that all photons from signal sources of interest will be used to update the state, but it also allows more background photons to be validated which in turn leads to a higher computational load.

8. Monte Carlo Simulations

In order to assess the feasibility of the techniques proposed here, a series of Monte Carlo simulations were performed. The details of the simulations are discussed below.

In these simulations, the orientation of the spacecraft was constrained to a single rotational degree of freedom. This simplification was chosen to allow the efficacy of the algorithms proposed to be analyzed in a simplified scenario before extending them to a full 6DOF estimator. As a result of this simulation, the reduced state vector consisted of the following values.

$$\hat{\mathbf{x}} = \begin{bmatrix} \hat{\mathbf{c}}_{\tilde{\lambda},S^0} \\ \hat{\mathbf{c}}_{\tilde{\lambda},S^1} \\ \vdots \\ \hat{\mathbf{c}}_{\tilde{\lambda},S^N} \\ \hat{\theta} \end{bmatrix} \tag{35}$$

At the initialization of each simulation, a scalar attitude and position were generated for the detector. In each simulation, the attitude of the detector was selected such that the detector was pointed at one of of several millisecond pulsars which have been previously identified as candidates for pulsar x-ray navigation.

The position of the detector, and therefore the TDOA of the photons was selected such that the TDOA would be within one period pulsar period of the pulsar at which the detector was pointing, so as to remove the phase ambiguity problem from the analysis.

A series of photon TOAs and AOAs were generated for the detector based on its position and orientation, and the surface area of the detector. Photons were generated based on the known characteristics of the pulsars. The TOA and AOA of the photons were determined based on the position and orientation of the detector. In addition, background photon arrivals were generated, based on the area and field-of-view of the detector and the ambient cosmic x-ray background flux levels. The background flux levels were computed using the equations presented in [19].

The filter was then initialized with a corrupted estimate of attitude, as follows.

$$\begin{aligned} \hat{\theta}_0 &= \mathcal{N}\left[\theta^{(p)}, \sigma_\theta^2\right] \\ \mathbf{P}_0 &= \sigma_\theta^2 \end{aligned} \tag{36}$$

The filter was initialized with no knowledge of the true TDOA.

The filter then processed the generated pulsar and background photons, and the final estimate of TDOA and attitude was stored. The filter used a validation threshold of $\gamma = 3$. Since the attitude was only estimated in one dimension, the validation threshold corresponds to a $\pm 3\sigma$ validation region, implying a 99.7% probability that photons from the signal source would be validated.

This process was repeated multiple times for each pulsar under consideration, with an array of detector areas. The standard deviation of the errors for each pulsar/detector area combination was then computed to determine the accuracy of the estimates.

Additional details of the simulations are given in Table 1. Details of the pulsars used in these simulations are given in Table 2.

8.1 Theoretical Accuracy

In order to compare the accuracies achieved by the estimation scheme proposed, the results of the Monte Carlo simulation are compared to the theoretical accuracy of TDOA estimation for an x-ray pulsar. The theoretical accuracy to which TDOA may be determined for a given pulsar is expressed as follows [3]:

$$\sigma_{TOA} = \frac{W}{2\text{SNR}} \tag{37a}$$

$$\text{SNR} = \frac{\lambda^{(p)} A_D p_f t_{\text{obs}}}{\sqrt{\left[\lambda^{(v)} + \lambda^{(p)}(1-p_f)\right]\left(A_D t_{\text{obs}} \frac{W}{T}\right) + \lambda^{(p)} A_D p_f t_{\text{obs}}}} \tag{37b}$$

where

- t_{obs} is the observation time
- p_f is the fraction of the photons that are part of the "pulsed" signal component
- W is the pulse width (full width at half maximum) in seconds
- T is the period of the pulsar
- A_D is the area of the detector
- $\lambda^{(S)}$ is the average photon flux from the pulsar
- $\lambda^{(v)}$ is the average photon flux from background noise

The expression above gives the expected accuracy to which a single TDOA could be computed, given an observation interval t_{obs}. The expression does not take into account the changing position of the observer during the observation, or that the velocity of the observer may not be perfectly known. Therefore, in order to perform a meaningful comparison between the estimation techniques discussed here and the theoretical accuracy, the zero-velocity case was chosen.

8.2 MLE Estimator

In addition to the filter proposed here, a maximum likelihood estimator was also used to compute the TDOA of the signal for each pulsar. The MLE used in these simulations was a simplified version of an "approximate MLE" presented in [11]. The estimator computes the maximum likelihood estimate of phase offset and frequency shift given an observation of N photons. The estimator is expressed in its full form as follows:

$$(\hat{\tau}, \hat{f}) = \text{argmax}_{\tau,f} \sum_{k=1}^{N} \log\lambda_O(\tilde{\phi}(T_k) + \tau + f(T_k - t_a)) \tag{38}$$

where

- T_k is the arrival time of the k^{th} photon
- $\hat{\tau}$ is the resulting ML estimate of time offset
- $\hat{f}$ is the resulting ML estimate of frequency shift
- $\tilde{\phi}(T_k)$ is the predicted phase, based on an initial estimate of the kinematic state of the vehicle from the navigation filter

In these simulations, the detector is assumed to be stationary (or equivalently, the velocity of the detector is assumed to be known perfectly). Consequently, the MLE estimator becomes:

$$\hat{\tau} = \text{argmax}_{\tau} \sum_{k=1}^{N} \log\lambda^{(O)}(T_k + \tau) \tag{39}$$

The ML estimate of TDOA was found using a grided search algorithm over possible TDOAs from zero to the pulsar period.

8.2.1 Photon Validation

The photons were validated for the MLE estimator in a similar manner to the validation technique used for the measurement updates. Specifically, photons falling within the 3σ bounds of the attitude residual variance based on the variance of the initial estimate were used, while photons that fell outside of those bounds were rejected.

$$0 \leq (\sigma_{0,\theta} + \mathbf{R}_{\boldsymbol{\alpha}}) \leq \gamma \tag{40}$$

$\mathbf{R_\alpha}$	t_{obs} (s)	Attitude $\pm 3\sigma_0(^\circ)$	Background Flux $\left(\frac{erg}{cm^2 s}\right)$	Detector FOV $(^\circ)$	Energy range (keV)	Simulations
1.0E-06	5000	0.3	1.3E-09	10	2 - 10	250
1.0E-06	5000	10.9	1.3E-09	10	2 - 10	250

Table 1: Monte Carlo Simulation Parameters

Flux $\left(\frac{erg}{cm^2 s}\right)$	Name	Period (s)	Pulse width	Pulsed fraction
1.71E-12	J0437-4715	0.005757	0.000091	0.27
5.36E-13	B1957+20	0.001607	0.000059	0.60
1.25E-12	B1821-24	0.003054	0.000053	0.98

Table 2: Pulsar Parameters [3, 20]

8.3 Simulation Results

Figures 2 and 3 show the standard deviation of TDOA estimates for the MSPs analyzed as a function of detector area. The plots include the standard deviation of the error of TDOA estimated using the algorithm presented here, as well as the standard deviation of TDOA estimated using the MLE. The plots also include the theoretical accuracy for the given area/pulsar/FOV combination, based on Equation 37. Finally, at the top of each sub-plot is a dashed line indicating the standard deviation of a uniform distribution with bounds equal to the pulsar period. This line indicates how accurately the pulsar period would be guessed if a value were picked at random.

Figures 4 and 5 show the standard deviation of the orientation estimate errors as a function of detector area. Since the MLE does not estimate attitude, there is only one estimated error to plot. Additionally, a theoretical lower bound was not derived, so none is shown. The dashed line at the top of the plots indicates the standard deviation of the initial attitude estimation error, $\sigma_{0,\theta}$.

Figures 2 and 4 contain the results from Monte Carlo simulations when the filter was initialized with an attitude error of $\sim$ 30mrad. This corresponds to a $\pm 3\sigma$ validation region of approximately 10 degrees.

Figures 3 and 5 contain the results from Monte Carlo simulations when the filter was initialized with an attitude error of $\sim$ 1mrad. This corresponds to a $\pm 3\sigma$ validation region of approximately 0.3 degrees.

9. Discussion

The results of the Monte Carlo simulations indicate that the algorithm proposed here is capable of jointly estimating TDOA and orientation of a detector from photon arrivals, in the simplified scenario that was simulated here. Some of the key findings of this study are discussed in more detail below.

9.1 Comparison to MLE

The results of the simulations performed indicate that the method proposed here is capable of outperforming an MLE-based TDOA estimator. The increase in accuracy of the estimator proposed here over the MLE method is due to the fact that this estimator recursively estimates attitude, and uses that attitude estimate to reject more background photons.

In contrast, the MLE uses only the initial estimate of attitude to reject background photons. Since the initial estimate of attitude is generally worse than the final estimate of attitude, the filter proposed here is capable of rejecting more background photons, particularly towards the end of the observation period when the estimator has converged on the correct attitude estimate.

9.2 Sensitivity to Initial Errors

The estimator proposed here is non-linear, and is highly sensitive to the quality of initial estimate. In particular, the estimator is sensitive to poor initial attitude estimates. Initial results indicate that the filter is generally able to converge on the correct attitude when the $\pm 3\sigma$ region of initial attitude covariance is less than the detector field-of-view.

9.3 Bias Toward Strong Signal

In addition to the sensitivity to initial attitude error discussed above, there is another phenomenon which manifests itself under certain conditions. This phenomenon is manifested as a tendency of the estimator to assign arriving photons to the brightest source within the validation region.

This phenomenon can be explained as follows. Suppose that there are two signal sources, signal A

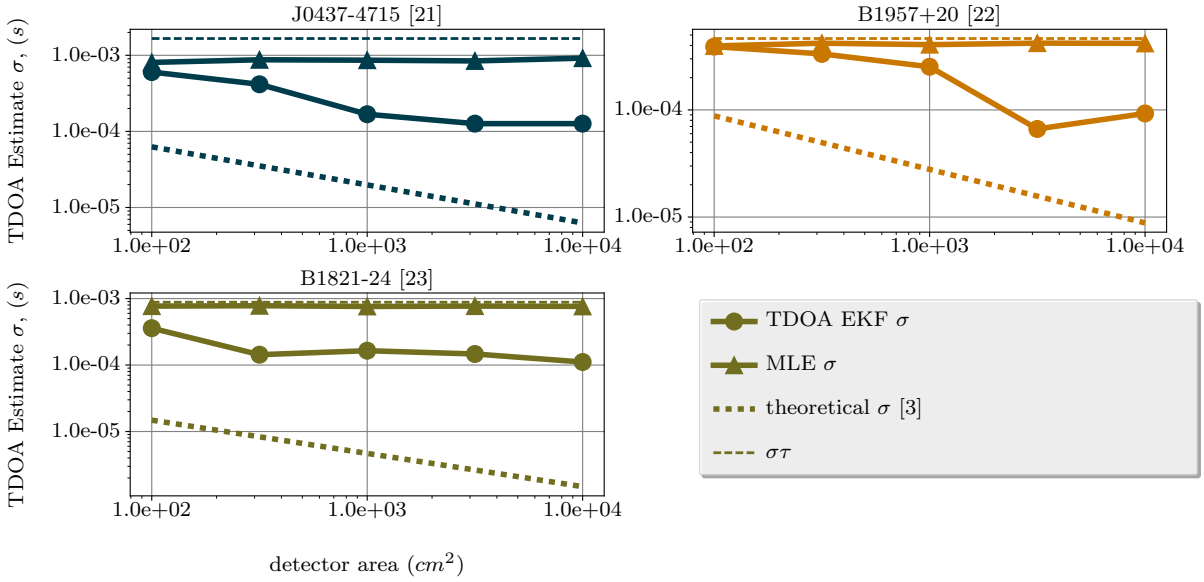

Fig. 2: TDOA Estimation Error Analysis, Large Initial Error

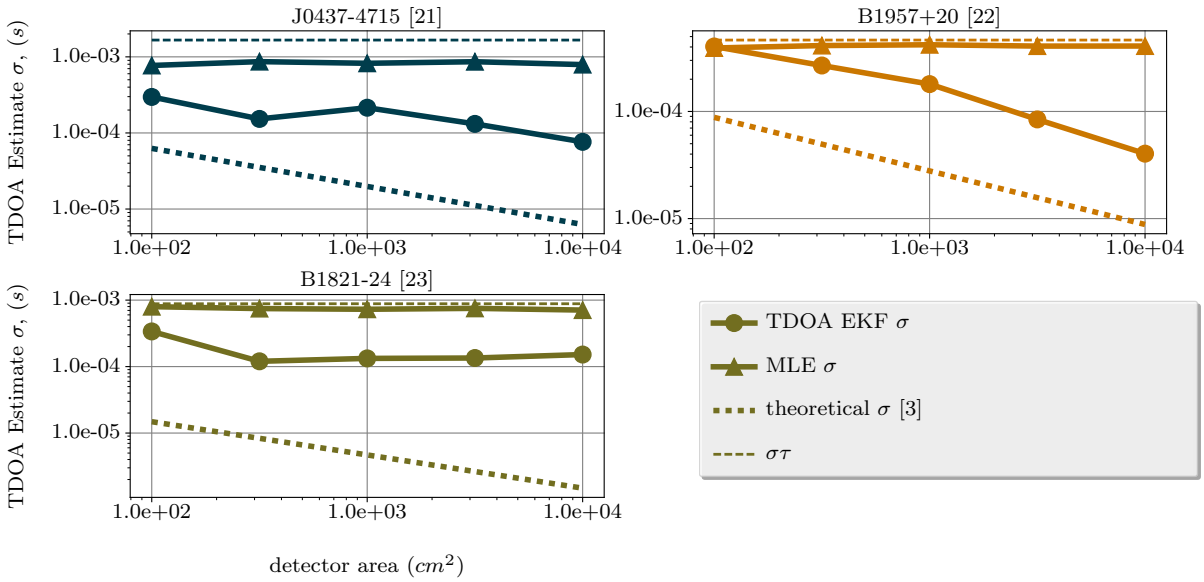

Fig. 3: TDOA Estimation Error Analysis, Small Initial Error

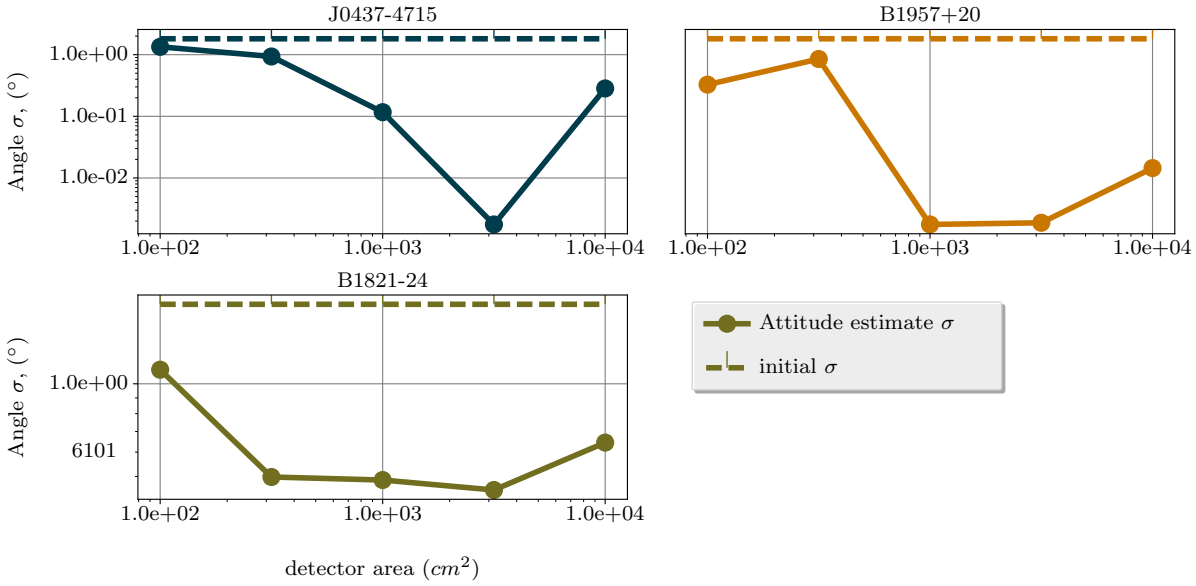

Fig. 4: Angle Estimation Error Analysis, Large Initial Error

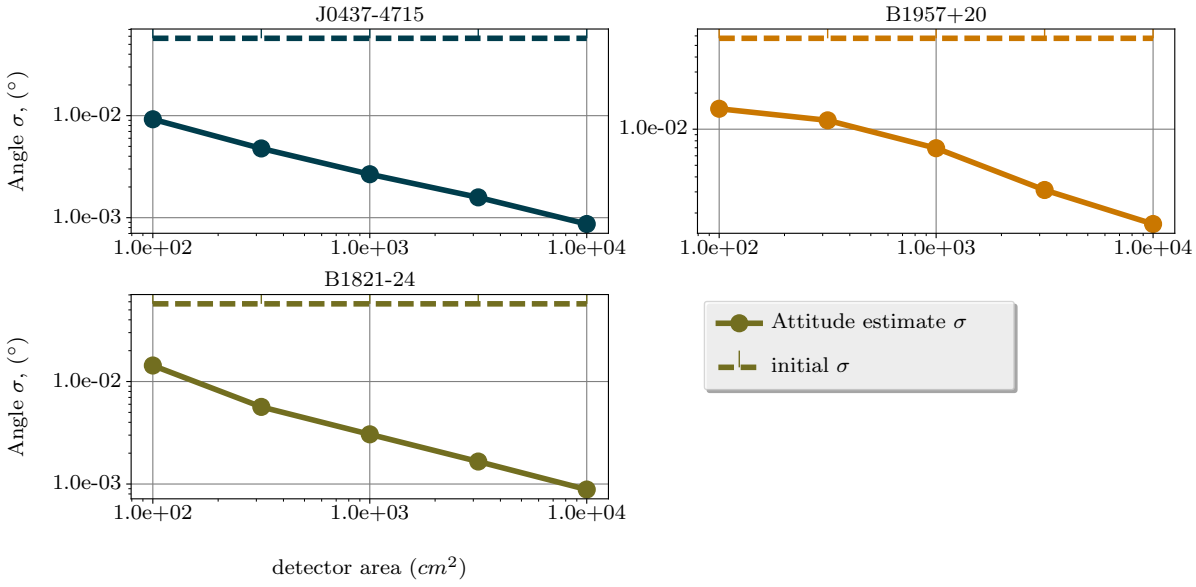

Fig. 5: Angle Estimation Error Analysis, Small Initial Error

and signal B. Suppose that attitude uncertainty is large enough that all photons hitting the detector fall within the $\pm 3\sigma$ validation region for both signal sources, and the angle-of-arrival probability is roughly equal for each signal source.

Suppose further that the position of the detector is poorly known, such that the time-of-arrival probability is also roughly equal for both signal sources. In this case, the only difference in the association probabilities for the two signal sources will be the relative signal strength of each source. Thus, the estimator will always compute a higher probability of association for whichever signal has a higher flux.

Put another way, if the detector has no idea which way it is pointing or where it is, then the most probable association event for every photon will *always* be with the signal source that has the highest flux. This divergence is the cause of some of the unexpectedly large attitude errors seen in some of the Monte Carlo simulations.

10. Conclusion

In this work, an estimator was derived to estimate position and orientation of a spacecraft from astrophysical signals of opportunity, in particular pulsars. The estimator is based on the Probabilistic Data Association Filter. Data association is one of the key challenges addressed in this filter. The probability of association with a given signal source based on time and angle of arrival was derived. That probability is then used in a vector-matching algorithm to estimate orientation, along with a time-difference of arrival algorithm to estimate position. The performance of the algorithm was analyzed with a series of Monte Carlo simulations, and the performance of the algorithm was compared to a maximum likelihood estimator for estimating time-difference of arrival. The algorithm proposed here was found to match or exceed the performance of the maximum likelihood estimator for a variety of initial conditions. Several limitations of the algorithm were also identified, particularly the filter's sensitivity to very low quality initial attitude estimates.

While the joint estimation scheme presented here is capable of producing higher quality position and attitude solutions in some cases, it suffers from some limitations. Particularly, the filter does not function well when initialized with very large attitude errors. This implies that an alternative estimation technique may be needed for initialization in "lost in space" situations, i.e. situations in which the detector has no prior knowledge of its position or attitude.

Acknowledgments

This research has made use of data obtained through the High Energy Astrophysics Science Archive Research Center Online Service, provided by the NASA/Goddard Space Flight Center. This research has made use of data obtained from the *Suzaku* satellite, a collaborative mission between the space agencies of Japan (JAXA) and the USA (NASA). The authors gratefully acknowledge JAXA/NASA for the data. The authors also acknowledge the NASA/Minnesota Space Grant Consortium and the Air Force Research Lab University Nanosat Program for providing funding to support this work. The authors also acknowledge the contributions of Dr. Lindsay Glesener in her assistance with obtaining and analyzing x-ray data and assessing the level of background noise to use in the simulation studies. While the authors gratefully acknowledge the aforementioned individuals and organizations, the views and conclusions expressed in this paper are those of the authors alone and should not be interpreted as necessarily representing the official policies, either expressed or implied, of any organization.

References

[1] D. S. Bagri and W. A. Majid, "Estimating accurate relative spacecraft angular position from deep space network very long baseline interferometry phases using X-band telemetry or differential one-way ranging tones," *The Interplanetary Network Progress Report*, vol. 42, no. 172, pp. 1–10, 2008. [Online]. Available: http://ipnpr.jpl.nasa.gov/progress_report/42-172/172B.pdf

[2] T. Ichikawa, "The angular position estimation for the moving spacecraft using two rotating tracking station," pp. 2293–2298, 2011.

[3] S. I. Sheikh and D. J. Pines, "Spacecraft Navigation Using X-Ray Pulsars," *Journal of Guidance, Control, and Dynamics*, vol. 29, no. 1, pp. 49–63, jan 2006. [Online]. Available: https://doi.org/10.2514/1.13331

[4] A. R. Golshan and S. I. Sheikh, "On pulse phase estimation and tracking of variable celestial X-ray sources," in *Institute of Navigation 63rd Annual Meeting*, no. April. Cambridge, MA: Institute of Navigation, 2007, pp. 413–422.

[5] J. Sala, A. Urruela *et al.*, "Feasibility study for a spacecraft navigation system relying on pulsar timing information," European Space Agency, Tech. Rep., 2004. [Online]. Available:

http://www.esa.int/gsp/ACT/doc/ARI/ARI Study Report/ACT-RPT-MAD-ARI-03-4202-Pulsar Navigation-UPC.pdf

[6] A. A. Emadzadeh, C. G. Lopes, and J. L. Speyer, "Online time delay estimation of pulsar signals for relative navigation using adaptive filters," in *2008 IEEE/ION Position, Location and Navigation Symposium*, IEEE. IEEE, 2008, pp. 714–719. [Online]. Available: http://ieeexplore.ieee.org/document/4570029/

[7] A. A. Emadzadeh and J. L. Speyer, "A new relative navigation system based on X-ray pulsar measurements," in *2010 IEEE Aerospace Conference*, IEEE. IEEE, mar 2010, pp. 1–8. [Online]. Available: http://ieeexplore.ieee.org/document/5446934/

[8] S. I. Sheikh, J. E. Hanson *et al.*, "Spacecraft Navigation and Timing Using X-ray Pulsars," *Navigation*, vol. 58, no. 2, pp. 165–186, jun 2011. [Online]. Available: http://doi.wiley.com/10.1002/j.2161-4296.2011.tb01799.x

[9] A. A. Emadzadeh and J. L. Speyer, "X-Ray Pulsar-Based Relative Navigation using Epoch Folding," *IEEE Transactions on Aerospace and Electronic Systems*, vol. 47, no. 4, pp. 2317–2328, 2011. [Online]. Available: http://ieeexplore.ieee.org/document/6034635/

[10] ——, "Relative Navigation Between Two Spacecraft Using X-ray Pulsars," *IEEE Transactions on Control Systems Technology*, vol. 19, no. 5, pp. 1021–1035, sep 2011. [Online]. Available: http://ieeexplore.ieee.org/document/5580018/

[11] L. M. B. Winternitz, M. A. Hassouneh *et al.*, "X-ray pulsar navigation algorithms and testbed for SEXTANT," in *2015 IEEE Aerospace Conference*, IEEE. Big Sky, MT, USA: IEEE, mar 2015, pp. 1–14. [Online]. Available: http://ieeexplore.ieee.org/document/7118936/

[12] J. T. Runnels and D. Gebre-Egziabher, "Recursive Range Estimation Using Astrophysical Signals of Opportunity," *Journal of Guidance, Control, and Dynamics*, vol. 40, no. 9, pp. 1–13, 2017. [Online]. Available: https://arc.aiaa.org/doi/10.2514/1.G002650

[13] C. S. Hisamoto and S. I. Sheikh, "Spacecraft Navigation Using Celestial Gamma-Ray Sources," *Journal of Guidance, Control, and Dynamics*, vol. 38, no. 9, pp. 1765–1774, sep 2015. [Online]. Available: http://arc.aiaa.org/doi/10.2514/1.G001008

[14] Y. Bar-Shalom, F. Daum, and J. Huang, "The probabilistic data association filter," *IEEE Control Systems Magazine*, vol. 29, no. 6, pp. 82–100, 2009.

[15] Y. Bar-Shalom and X.-R. Li, "Multiple Targets in Clutter: Bayesian Approaches," in *Multitarget-Multisensor Tracking*, 1st ed. Storrs, Connecticut: Yaakov Bar-Shalom, 1995, ch. 6, pp. 307–372.

[16] V. Bageshwar, D. Gebre-Egziabher *et al.*, "Inertially-Aided Vector Matching Algorithm for Attitude Determination of Spin Stabilized Satellite," in *AIAA Guidance, Navigation and Control Conference and Exhibit*, no. August. Reston, Virigina: American Institute of Aeronautics and Astronautics, aug 2008. [Online]. Available: http://arc.aiaa.org/doi/10.2514/6.2008-6295

[17] C. Lewis, P. A. W. (Naval Postgraduate School, Monterey and C. Shedler, G. S. (IBM Research Laboratory, San Jose, "Simulation of nonhomogenous Poisson processes by thinning," *Naval Research Logistic Quarterly*, vol. 26, no. 42, pp. 403–414, 1979.

[18] Y. Bar-Shalom, X.-R. Li, and T. Kirubarajan, *Estimation with Applications to Tracking and Navigation*, 1st ed. Hoboken, NJ: John Wiley & Sons, Inc, 2001.

[19] D. E. Gruber, J. L. Matteson *et al.*, "The Spectrum of Diffuse Cosmic Hard X-Rays Measured with HEAO 1," *The Astrophysical Journal*, vol. 520, no. 1, pp. 124–129, 1999. [Online]. Available: http://iopscience.iop.org/0004-637X/520/1/124/fulltext/

[20] J. P. Halpern, C. Martin, and H. L. Marshall, "Soft X-Ray Properties of the Binary Millisecond Pulsar J0437-4715," *The Astrophysical Journal*, vol. 462, p. 908, may 1996. [Online]. Available: http://adsabs.harvard.edu/doi/10.1086/177204

[21] A. A. Abdo, M. Ackermann *et al.*, "Fermi Large Area Telescope First Source Catalog," *The Astrophysical Journal Supplement Series*, vol. 188, no. 2, pp. 405–436, 2010. [Online]. Available: http://stacks.iop.org/0067-0049/188/i=2/a=405

[22] L. Guillemot, T. J. Johnson *et al.*, "Pulsed Gamma Rays from the Original Millisecond and Black Widow Pulsars: A Case for Caustic

Radio Emission?" *The Astrophysical Journal*, vol. 744, no. 1, p. 33, 2012.

[23] T. J. Johnson, L. Guillemot *et al.*, "Broadband Pulsations from PSR B1821-24: Implications for Emission Models and the Pulsar Population of M28," *The Astrophysical Journal*, vol. 778, no. 2, p. 106, 2013.